J|A|C|S
ARTICLES
Published on Web 07/12/2005

A Joint Experimental and Theoretical Study of Cation−π Interactions: Multiple-Decker Sandwich Complexes of Ferrocene with Alkali Metal Ions (Li^+, Na^+, K^+, Rb^+, Cs^+)

Alireza Haghiri Ilkhechi,[†] Jose M. Mercero,[‡] Iñaki Silanes,[‡] Michael Bolte,[†] Matthias Scheibitz,[†] Hans-Wolfram Lerner,[†] Jesus M. Ugalde,*[,‡] and Matthias Wagner*[,†]

Contribution from the Institut für Anorganische Chemie, J.W. Goethe-Universität Frankfurt, Marie-Curie-Strasse 11, D-60439 Frankfurt (Main), Germany, and Kimika Fakultatea, Euskal Herriko Unibertsitatea, and Donostia International Physics Center DIPC, P. K. 1072, 20080 Donostia Euskadi, Spain

Received March 10, 2005; E-mail: matthias.wagner@chemie.uni-frankfurt.de; ugalde@sq.ehu.es

Abstract: A systematic study of cation−π interactions between alkali metal ions and the cyclopentadienyl ring of ferrocene is presented. The alkali metal (Li^+, Na^+, K^+, Rb^+, Cs^+) salts of the ditopic mono(pyrazol-1-yl)borate ligand $[1,1'\text{-fc}(BMe_2pz)_2]^{2-}$ crystallize from dimethoxyethane as multiple-decker sandwich complexes with the M^+ ions bound to the π faces of the ferrocene cyclopentadienyl rings in an η^5 manner (fc = $(C_5H_4)_2Fe$; pz = pyrazolyl). X-ray crystallography of the lithium complex reveals discrete trimetallic entities with each lithium ion being coordinated by only one cyclopentadienyl ring. The sodium salt forms polyanionic zigzag chains where each Na^+ ion bridges the cyclopentadienyl rings of two ferrocene moieties. Linear columns $[-CpR-Fe-CpR-M^+-CpR-Fe-CpR-M^+-]_\infty$ (R = $[-BMe_2pz]^-$) are established by the K^+, Rb^+, and Cs^+ derivatives in the solid state. According to DFT calculations, the binding enthalpies of $M^+-\eta^5$(ferrocene) model complexes are about 20% higher as compared to the corresponding $M^+-\eta^6$-(benzene) aggregates when $M^+ = Li^+$ or Na^+. For K^+ and Rb^+, the degree of cation−π interaction with both aromatics is about the same. The binding sequence along the $M^+-\eta^5$(ferrocene) series follows a classical electrostatic trend with the smaller ions being more tightly bound.

Introduction

Alkali metal cations, as well as tetraalkylammonium groups, are attracted to the π face of aromatic structures through a strong noncovalent binding force. During the past 20 years, both experimental and theoretical evidence has been gathered that suggests these cation−π interactions play a prominent role in various areas of chemistry and biology.[1−5] For example, cation−π interactions appear to contribute to the ion selectivity in potassium channels,[6] they are important for the binding of acetylcholine to the active site of the enzyme acetylcholine esterase,[7] and they guide the stereoselective cyclization of squalene epoxide in the enzymatically catalyzed process of steroid biosynthesis.[7] Even though cation−π interactions involving arene molecules have been studied extensively, only very little is known about the degree of cation binding to organometallic structures such as the cyclopentadienyl ring of sandwich complexes. In this context, ferrocene, being the prototypical sandwich complex and said to be even more aromatic than benzene,[8] is of particular interest for further studies.[9] This is more so as ferrocene-based planar-chiral ligands and ferrocenyl-substituted crown ethers are important in homogeneous catalysis and alkali metal complexation, respectively.[10] In both cases, it may be interesting to explore the potential of cation−π interactions involving the ferrocene cyclopentadienyl rings for the design of improved ligand systems and redox-switchable alkali metal receptors.

The main focus of this paper is on the role of cation−π interactions for the development of ferrocene-containing multiple-decker sandwich complexes. Even though $[Fe_2(C_5H_5)_3]^+$ and clusters of the general formula $V_n[Fe(C_5H_5)_2]_{n+1}$ ($n = 1-3$) have been detected in the gas phase,[11,12] it was for a long time not possible to stabilize any of these aggregates in the condensed phase. In 1998, Laguna et al. reported on a double sandwich

[†] J.W. Goethe-Universität Frankfurt.
[‡] Euskal Herriko Unibertsitatea, and Donostia International Physics Center DIPC.

(1) Schade, C.; Schleyer, P. v. R. *Adv. Organomet. Chem.* **1987**, *27*, 169−278.
(2) Ma, J. C.; Dougherty, D. A. *Chem. Rev.* **1997**, *97*, 1303−1324.
(3) Gokel, G. W.; Wall, S. L. D.; Meadows, E. S. *Eur. J. Org. Chem.* **2000**, 2967−2978.
(4) Gokel, G. W.; Barbour, L. J.; Wall, S. L. D.; Meadows, E. S. *Coord. Chem. Rev.* **2001**, *222*, 127−154.
(5) Gokel, G. W.; Barbour, L. J.; Ferdani, R.; Hu, J. *Acc. Chem. Res.* **2002**, *35*, 878−886.
(6) Kumpf, R. A.; Dougherty, D. A. *Science* **1993**, *261*, 1708−1710.
(7) Dougherty, D. A. *Science* **1996**, *271*, 163−168.
(8) Laskoski, M.; Steffen, W.; Smith, M. D.; Bunz, U. H. F. *Chem. Commun.* **2001**, 691−692.
(9) Irigoras, A.; Mercero, J. M.; Silanes, I.; Ugalde, J. M. *J. Am. Chem. Soc.* **2001**, *123*, 5040−5043.
(10) Togni, A.; Hayashi, T., *Ferrocenes*; VCH: Weinheim, 1995.
(11) Schildcrout, S. M. *J. Am. Chem. Soc.* **1973**, *95*, 3846−3849.
(12) Nagao, S.; Kato, A.; Nakajima, A.; Kaya, K. *J. Am. Chem. Soc.* **2000**, *122*, 4221−4222.

10.1021/ja051544+ CCC: $30.25

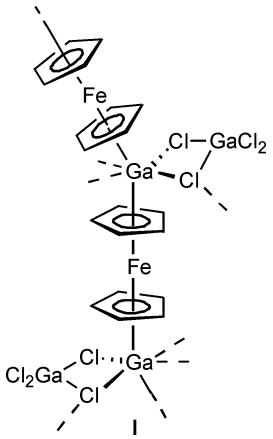

Figure 1. A Ga^+-ferrocene multiple-decker sandwich complex **I**.

silver(I) complex with 1,1′-bis(diethyldithiocarbamate)ferrocene. This ligand-supported polymer represented the first isolable compound where an η^5-cyclopentadienyl ring of ferrocene was shared with another metal atom via the π system.[13] More recently, Enders et al. synthesized the $ZnCl_2$ complex of η^5-1-(8-quinolyl)-2,3,4,5-tetramethylcyclopentadienyl-η^5-cyclopentadienyliron in which the zinc ion is surrounded tetrahedrally by two chlorine atoms, the nitrogen atom of the 8-quinolyl sidearm, and one carbon atom of the tetramethylcyclopentadienyl ring.[14] Our group published the synthesis and X-ray crystal structure analysis of compound **I** (Figure 1) consisting of a ligand-unsupported array of alternating Ga(I) and Fe(II) ions connected by η^5,μ-$[C_5H_5]^-$ moieties.[15]

According to density functional (DFT) calculations, the binding energy of two ferrocenes to Ga^+ is about 20 kcal mol^{-1} higher than that for the formation of $[Ga(C_6H_6)_2]^+$ from Ga^+ and two benzene molecules. Fragment analysis of $\{[Fe(C_5H_5)_2]_2$-$Ga\}^+$ indicated a transfer of 0.4 electrons into the gallium 4p orbitals as compared to a zero occupancy for the isolated ion. These encouraging results prompted us to start a systematic search for more one-dimensional solids exhibiting the structural motif of ferrocene-containing multiple-decker sandwich complexes. It is important to note in this context that the synthesis protocol developed for the ligand-unsupported polymer **I**[15] is unique in that it starts from the covalent molecule $GaCl_3$, which readily dissolves in noncoordinating solvents. For a more general approach, it will become necessary to use ionic metal salts that usually require strongly coordinating solvents as reaction media. We therefore decided to follow Laguna's approach and employ ferrocene derivatives equipped with Lewis-basic substituents designed to stabilize the aimed-for metal···Cp interactions.

Ferrocene- and cymantrene-based tris(pyrazol-1-yl)borate (scorpionate) ligands **II**[16,17] and **III**[18] (Figure 2) are readily available and have been used for the preparation of heterooligonuclear transition metal complexes.[19−21]

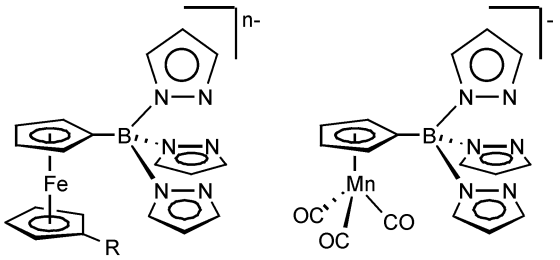

IIa: R = H, n = 1 **III**
IIb: R = Bpz_3, n = 2

Figure 2. Ferrocene- and cymantrene-based tris(pyrazol-1-yl)borate derivatives **II** and **III**.

Scheme 1. Synthesis of $\mathbf{2M}_2$ ($M^+ = Li^+, Na^+, K^+, Rb^+, Cs^+$); (i) +2 Mpz, Et_2O, −78 °C

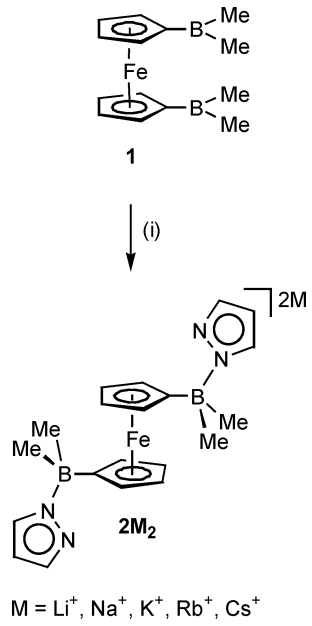

M = Li^+, Na^+, K^+, Rb^+, Cs^+

Cyclic voltammetric measurements on $(\mathbf{IIa})ML_n$ and $(\mathbf{IIa})_2M$ revealed the oxidation state of the ferrocenyl substituent(s) to have a significant influence on the redox potential of M and vice versa. Notably, the heterotrinuclear complex $(\mathbf{IIa})_2Cu$ exhibits two well-resolved Fe(II)/Fe(III) redox waves, thereby indicating an electronic communication between the two ferrocenyl substituents. Starting from the ditopic scorpionate ligand **IIb** and divalent transition metal ions, polymers of the general formula $[(\mathbf{IIb})M]_n$ are accessible. In an attempt to further increase the degree of metal−metal interaction along the chain and to promote direct bonding between the ferrocenyl Cp rings and the coordinated metal atom,[22] the *tris*(pyrazol-1-yl)borate substituents of **IIb** (Figure 2) are now replaced by *mono*(pyrazol-1-yl)borate fragments, thereby creating the novel ligand $[\mathbf{2}]^{2-}$ (Scheme 1).

In the following, we report on the synthesis and structural characterization of the complete series $\mathbf{2Li}_2$, $\mathbf{2Na}_2$, $\mathbf{2K}_2$, $\mathbf{2Rb}_2$, $\mathbf{2Cs}_2$ and give some insight into the different structural effects

(13) Crespo, O.; Gimeno, M. C.; Jones, P. G.; Laguna, A.; Sarroca, C. *Chem. Commun.* **1998**, 1481−1482.
(14) Enders, M.; Ludwig, G.; Pritzkow, H. *Organometallics* **2002**, *21*, 3856−3859.
(15) Scholz, S.; Green, J. C.; Lerner, H.-W.; Bolte, M.; Wagner, M. *Chem. Commun.* **2002**, 36−37.
(16) Jäkle, F.; Polborn, K.; Wagner, M. *Chem. Ber.* **1996**, *129*, 603−606.
(17) Herdtweck, E.; Peters, F.; Scherer, W.; Wagner, M. *Polyhedron* **1998**, *17*, 1149−1157.
(18) Guo, S. L.; Bats, J. W.; Bolte, M.; Wagner, M. *J. Chem. Soc., Dalton Trans.* **2001**, 3572−3576.
(19) Fabrizi de Biani, F.; Jäkle, F.; Spiegler, M.; Wagner, M.; Zanello, P. *Inorg. Chem.* **1997**, *36*, 2103−2111.
(20) Guo, S. L.; Peters, F.; Fabrizi de Biani, F.; Bats, J. W.; Herdtweck, E.; Zanello, P.; Wagner, M. *Inorg. Chem.* **2001**, *40*, 4928−4936.
(21) Haghiri Ilkhechi, A.; Guo, S. L.; Bolte, M.; Wagner, M. *Dalton Trans.* **2003**, 2303−2307.
(22) Haghiri Ilkhechi, A.; Scheibitz, M.; Bolte, M.; Lerner, H.-W.; Wagner, M. *Polyhedron* **2004**, *23*, 2597−2604.

exerted by coordinated dimethoxyethane (DME) and tetrahydrofurane (THF) molecules. The experimental investigations are augmented with density functional (DFT) calculations on model complexes between ferrocene and alkali metal ions ($M^+ = Li^+$, Na^+, K^+, Rb^+) to get deeper insight into the nature of the interaction between these two components.

Results and Discussion

Syntheses and NMR-Spectroscopic Characterization. Upon treatment of 1,1′-bis(dimethylboryl)ferrocene **1** with 2 equiv of the appropriate alkali metal pyrazolide (Mpz) in diethyl ether, the respective complexes $\mathbf{2M}_2\cdot(Et_2O)_x$ ($M^+ = Li^+$, Na^+, K^+, Rb^+, Cs^+) readily precipitate from the reaction mixtures (Scheme 1). X-ray quality crystals of $\mathbf{2M}_2\cdot(THF)_4$ ($M^+ = Na^+$, K^+, Rb^+) were obtained from THF at −30 °C, room temperature, and 5 °C, respectively. Recrystallization of $\mathbf{2Li}_2\cdot(Et_2O)_4$, $\mathbf{2M}_2\cdot(THF)_4$ ($M^+ = Na^+$, K^+, Rb^+), and crude $\mathbf{2Cs}_2\cdot(Et_2O)_x$ from DME gave single-crystalline materials of the composition $\mathbf{2Li}_2\cdot(DME)_2$ and $\mathbf{2M}_2\cdot(DME)_3$ ($M^+ = Na^+$, K^+, Rb^+, Cs^+). The complexes $\mathbf{2K}_2\cdot(THF)_4$, $\mathbf{2Rb}_2\cdot(THF)_4$, and $\mathbf{2Cs}_2\cdot(Et_2O)_x$ are only poorly soluble in DME. Elevated temperatures and the use of an ultrasonic bath were thus required to prepare saturated solutions.

All NMR spectra were run at ambient temperature in d_8-THF. The ^{11}B NMR resonances of $\mathbf{2M}_2$ lie in the range between −9.4 ppm ($\mathbf{2K}_2$) and −7.6 ppm ($\mathbf{2Rb}_2$, $\mathbf{2Cs}_2$), thereby testifying to the presence of tetracoordinated boron nuclei.[23] Both in the ^1H and in the ^{13}C NMR spectra, the two fragments [$C_5H_4B(Me_2)$-pz] of $\mathbf{2M}_2$ give rise to six signals only (C_5H_4−C*ipso* is generally not observed as a result of quadrupolar broadening[23]). This leads to the conclusion that there are no restrictions to intramolecular motion on the NMR time scale as was also observed for the quinolylferrocene−$ZnCl_2$[14] complex mentioned above. Moreover, no systematic changes of the C_5H_4 chemical shift values, which might indicate metal···Cp coordination in solution, are evident from a comparison of the NMR spectra of $\mathbf{2Li}_2$, $\mathbf{2Na}_2$, $\mathbf{2K}_2$, $\mathbf{2Rb}_2$, and $\mathbf{2Cs}_2$. At room temperature, the ^7Li NMR spectrum of $\mathbf{2Li}_2$ reveals one broad resonance at $\delta(^7Li) = -1.30$ ($h_{1/2} = 37$ Hz). A comparison with the chemical shift values of LiCl in d_8-THF before ($\delta(^7Li) = -1.54$; $h_{1/2} = 0.6$ Hz) and after ($\delta(^7Li) = -1.26$; $h_{1/2} = 0.6$ Hz) the addition of 1 equiv of pyrazole suggests that the Li^+ ion of $\mathbf{2Li}_2$ is mainly coordinated by solvent molecules in THF solution but that some interaction with the pyrazolyl substituent still remains. The large width at half-height of the ^7Li NMR resonance of $\mathbf{2Li}_2$ indicates a dynamic process to go on which possesses a significantly different rate constant or is even absent in the case of the Li^+−pyrazole complex. Upon cooling to −78 °C, the resonance is gradually shifted from −1.30 to −0.83 ppm and the signal becomes narrower ($h_{1/2} = 26$ Hz). Moreover, two minor additional species are now detected ($\delta(^7Li) = 0.68, 1.38$), which disappear again when the sample is allowed to approach room temperature.

Electrochemical Investigations. In THF solution, $\mathbf{2Li}_2\cdot(DME)_2$ gives rise to one ferrocenylene-centered oxidation with an Fe(II)/Fe(III) redox potential of $E^{\circ\prime} = -0.99$ V (vs FcH/FcH^+). An analysis of the cyclic voltammogram measured at room temperature with scan rates varying from 0.05 to 1.00 V s^{-1} not only confirms the chemical reversibility of the one-electron oxidation (i_{pc}/i_{pa} constantly equal to 1), but also proves its electrochemical reversibility (ΔE_p constantly close to 60 mV), thereby suggesting that no significant structural reorganization occurs upon electron removal. It is revealing to compare the redox potential of $\mathbf{2Li}_2\cdot(DME)_2$ with the electrochemical data of the dianionic [1.1]diborataferrocenophane $[\{Fe(C_5H_4)_2\}_2(BMe_2)_2]^{2-}$ ($E^{\circ\prime} = -1.02$ V, −1.33 V)[24] and of the neutral boron−nitrogen adduct $Fe(C_5H_4BMe_2\cdot DMAP)_2$ ($E^{\circ\prime} = -0.64$ V; DMAP: 4-(dimethylamino)pyridine).[25] In all three cases, the introduction of tetracoordinated substituents into the ferrocene core leads to a substantial cathodic shift of the Fe(II)/Fe(III) transition. As to be expected for electrostatic reasons, this effect is more pronounced for negatively charged borate groups than for neutral side chains. Moreover, the borate substituents of $[\mathbf{2}]^{2-}$ are obviously weaker electron donors than those in $[\{Fe(C_5H_4)_2\}_2(BMe_2)_2]^{2-}$, which is most likely due to the high group electronegativity of the pyrazolyl ring [cf. $Fe(C_5H_4B(pz)_3Tl)_2$: $E^{\circ\prime} = -0.02$ V].[19]

X-ray Crystal Structure Determinations. $\mathbf{2Li}_2\cdot(DME)_2$ crystallizes in the triclinic space group *P*-1. The asymmetric unit contains two complete and two half-molecules, which are both located on a center of inversion. As a result, there are six molecules in the unit cell. Because the structural parameters of all of the molecules are rather similar, only one of them is plotted in Figure 3.

$\mathbf{2Li}_2\cdot(DME)_2$ forms heterotrimetallic aggregates in the solid state (Figure 3). Each Li^+ ion is bonded to one chelating DME molecule and to the nitrogen lone-pair of one pyrazolyl sidearm, which places it on-top of the cyclopentadienyl ring. As a consequence, short distances are established between the Li^+ cations and the geometric centers (COG) of the cyclopentadienyl rings (Li(1)···COG(1) = 2.26 Å, Li(2)···COG(2) = 2.32 Å; the corresponding distances in the other three molecules are 2.26, 2.44, 2.30, and 2.51 Å; mean value: 2.35 Å). As the internal angles of the C(Cp)−B−N−N−Li chains do not depart appreciably from the ideal values of 109° and 120°, the molecular framework is apparently not suffering from internal strain.

The crystal lattice of the sodium derivative $\mathbf{2Na}_2\cdot(DME)_3$ (orthorhombic space group *Pbca*) consists of polyanionic zigzag chains $[\mathbf{2}Na]_n^{n-}$ and distorted octahedral $[Na(DME)_3]^+$ counterions (Figure 4). A major difference in the overall conformation of the ferrocene ligand $[\mathbf{2}]^{2-}$ in $\mathbf{2Na}_2\cdot(DME)_3$ and $\mathbf{2Li}_2\cdot(DME)_2$ lies in the torsion angle C(11)−COG(1)−COG(2)−C(21), which possesses values of −135.4° and 178.8°, respectively. Within the zigzag chains, each Na^+ ion binds to two pyrazolyl substituents of adjacent $[\mathbf{2}]^{2-}$ ligands and establishes short contacts to two cyclopentadienyl rings (Na(1)···COG($1^{\#}$) = 2.561 Å, Na(1)···COG(2) = 2.590 Å). Thus, the polymeric subunit $[\mathbf{2}Na]_n^{n-}$ can be regarded as a bent multiple-decker sandwich complex of ferrocene with sodium ions (dihedral angle C($11^{\#}$)C($12^{\#}$)C($13^{\#}$)C($14^{\#}$)C($15^{\#}$)//C(21)C(22)C(23)C(24)C(25) = 48.0°).

The complexes of the heavier alkali metal ions, $\mathbf{2K}_2\cdot(DME)_3$ (triclinic, *P*-1), $\mathbf{2Rb}_2\cdot(DME)_3$ (triclinic, *P*-1), and $\mathbf{2Cs}_2\cdot(DME)_3$

(23) Nöth, H.; Wrackmeyer, B. Nuclear Magnetic Resonance Spectroscopy of Boron Compounds. In *NMR Basic Principles and Progress*; Diehl, P., Fluck, E., Kosfeld, R., Eds.; Springer: Berlin, Heidelberg, New York, 1978.

(24) Scheibitz, M.; Winter, R. F.; Bolte, M.; Lerner, H.-W.; Wagner, M. *Angew. Chem., Int. Ed.* **2003**, *42*, 924−927.

(25) Fontani, M.; Peters, F.; Scherer, W.; Wachter, W.; Wagner, M.; Zanello, P. *Eur. J. Inorg. Chem.* **1998**, 1453−1465.

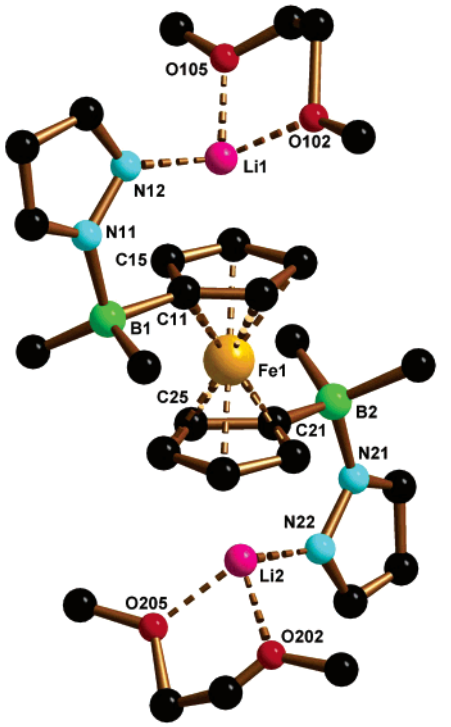

Figure 3. Molecular structure of **2Li**$_2$·(DME)$_2$ (hydrogen atoms omitted for clarity); selected bond lengths [Å] and angles [deg]: Li(1)···COG(1) = 2.26, Li(2)···COG(2) = 2.32, Li(1)−N(12) = 2.04(3), Li(2)−N(22) = 1.98(3); C(11)−B(1)−N(11) = 100.4(15), C(21)−B(2)−N(21) = 108.2(16), B(1)−N(11)−N(12) = 123.6(13), N(11)−N(12)−Li(1) = 124.2(11), B(2)−N(21)−N(22) = 122.3(14), N(21)−N(22)−Li(2) = 123.0(13); C(12)−C(11)−B(1)−N(11) = 98(2), C(22)−C(21)−B(2)−N(21) = 81.3(19), B(1)−N(11)−N(12)−Li(1) = −6(2), B(2)−N(21)−N(22)−Li(2) = 2(2).

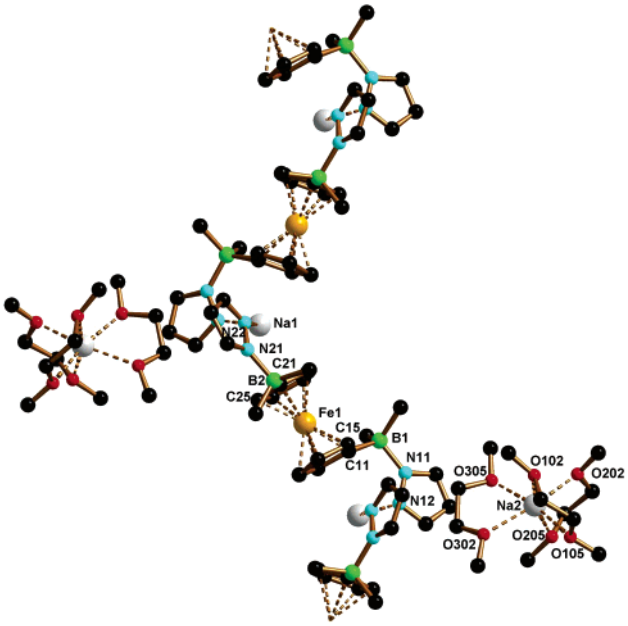

Figure 4. Molecular structure of **2Na**$_2$·(DME)$_3$ (hydrogen atoms omitted for clarity); selected bond lengths [Å] and angles [deg]: Na(1)···COG(1$^{\#}$) = 2.561, Na(1)···COG(2) = 2.590, Na(1)−N(12$^{\#}$) = 2.382(5), Na(1)−N(22) = 2.405(6); N(12$^{\#}$)−Na(1)−N(22) = 122.2(2). Symmetry transformation used to generate equivalent atoms: $x - {}^1/_2$, y, $-z + {}^1/_2$ (#).

(monoclinic, *C*2/*c*), are largely isostructural. Representative for these three compounds, the molecular structure of **2K**$_2$·(DME)$_3$ is depicted in Figure 5. In contrast to the bent polymer **2Na**$_2$·(DME)$_3$, linear columns of alternating ferrocene units and alkali

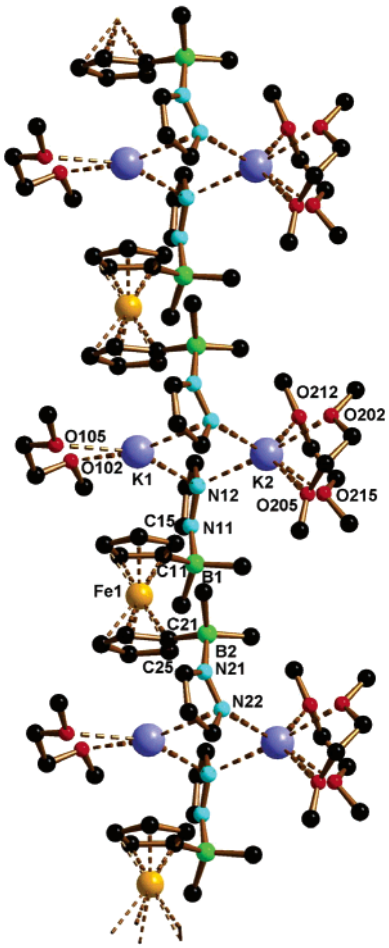

Figure 5. Molecular structure of **2K**$_2$·(DME)$_3$ (hydrogen atoms omitted for clarity); selected bond lengths [Å] and angles [deg]: K(1)···COG(1) = 3.228, K(1)···COG(2$^{\#}$) = 3.298; B(1)−N(11)−N(12)−K(1) = −66.0(4), B(1)−N(11)−N(12)−K(2) = 47.3(4), B(2)−N(21)−N(22)−K(1*) = −86.3(3), B(2)−N(21)−N(22)−K(2*) = 10.1(6). Symmetry transformation used to generate equivalent atoms: $x - 1$, y, z (#), $x + 1$, y, z (*). Molecular structure of **2Rb**$_2$·(DME)$_3$: Rb(1)···COG(1) = 3.285, Rb(1)···COG(2*) = 3.265; B(1)−N(11)−N(12)−Rb(1) = 68.3(13), B(1)−N(11)−N(12)−Rb(2) = −43.9(15), B(2)−N(21)−N(22)−Rb(1$^{\#}$) = 86.2(11), B(2)−N(21)−N(22)−Rb(2$^{\#}$) = −11.4(18). Symmetry transformation used to generate equivalent atoms: $x - 1$, y, z (#), $x + 1$, y, z (*). Molecular structure of **2Cs**$_2$·(DME)$_3$: Cs(1)···COG(1) = 3.283; B(1)−N(11)−N(12)−Cs(1) = −90.3(3), B(1)−N(11)−N(12)−Cs(2) = 12.0(7).

metal ions are established by the complexes of the higher homologues in the solid state (dihedral angle between the cyclopentadienyl rings of adjacent ferrocenylene fragments: 2.7° (**2K**$_2$·(DME)$_3$), 2.5° (**2Rb**$_2$·(DME)$_3$), 1.7° (**2Cs**$_2$·(DME)$_3$)). The conformation of the ferrocenylene fragments in **2K**$_2$·(DME)$_3$ (C(11)−COG(1)−COG(2)−C(21) = 92.1°; corresponding value in **2Rb**$_2$·(DME)$_3$, −93.2°, **2Cs**$_2$·(DME)$_3$, 86.7°) leads to a closer approach of its boryl substituents as compared to **2Na**$_2$·(DME)$_3$ (C(11)−COG(1)−COG(2)−C(21) = −135.4°) and **2Li**$_2$·(DME)$_2$ (C(11)−COG(1)−COG(2)−C(21) = 178.8°). Moreover, the pyrazolyl substituents now adopt bridging positions between two alkali metal ions M(1) and M(2). In the case of **2K**$_2$·(DME)$_3$ and **2Rb**$_2$·(DME)$_3$, one pyrazolyl bridge is roughly symmetric, while the other pyrazolyl ring binds in a π,σ-fashion to the two alkali metal ions. The latter coordination mode is also apparent in **2Cs**$_2$·(DME)$_3$. In addition to the pyrazolyl moieties, M(1) is bonded to one DME molecule and two cyclopentadienyl rings, whereas the coordination sphere of M(2)

is completed by two DME ligands. The distances between M(1) and the geometric centers of the neighboring C_5H_4 ligands are 3.228 Å/3.298 Å (K(1)), 3.265 Å/3.285 Å (Rb(1)), and 3.283 Å/3.283 Å (Cs(1)). Apart from $\mathbf{2K_2}\cdot(DME)_3$ there is only one example of an η^5-ferrocene−K^+ complex known in the literature, $[K(ferrocene)_2(toluene)_2]^+[Mg(HMDS)_3]^-$ (HMDS = hexamethyldisilazide).[26] Here, the cationic moiety consists of a potassium ion coordinated by the centroids of two toluene π systems and two ferrocenyl cyclopentadienyl rings in a distorted-tetrahedral geometry with a bond angle COG(FcH(1))−K^+−COG(FcH(2)) of 106.1° (FcH = ferrocene; cf. COG(FcH(1))−Na^+−COG(FcH(2)) = 132.0° in the bent polymer $\mathbf{2Na_2}\cdot(DME)_3$).

The average distance $K^+\cdots$COG(FcH) in $[K(ferrocene)_2(toluene)_2]^+$ equals 2.964 Å, 0.3 Å (about 10%) shorter than the corresponding value in $\mathbf{2K_2}\cdot(DME)_3$ (3.263 Å), which more closely approaches the $K^+\cdots COG(C_6H_5)$ distance of $[K(ferrocene)_2(toluene)_2]^+$ (3.143 Å). Several reasons can be suggested for the difference in the $K^+\cdots$ferrocene bond lengths of $[K(ferrocene)_2(toluene)_2]^+$ and $\mathbf{2K_2}\cdot(DME)_3$: (i) the $B(Me)_2pz$ sidearm may not be perfectly adjusted to the geometric requirements of the aggregate, (ii) the bulky DME molecule at K(1) can be expected to push the ferrocenylene moieties away from the alkali metal ion, (iii) the oxygen and nitrogen donors may lower the net positive charge of K^+ to such an extent that the $K^+\cdots$ferrocene π interaction is weakened, and (iv) in contrast to $[K(ferrocene)_2(toluene)_2]^+$, which features only one K^+ ion bonded to the ferrocene molecule, two potassium ions have to share the electron density provided by the ferrocenylene fragment in $\mathbf{2K_2}\cdot(DME)_3$.

As in the case of $\mathbf{2M_2}\cdot(DME)_3$ (M^+ = Na^+, K^+, Rb^+, Cs^+), polymeric aggregates are observed for $\mathbf{2Na_2}\cdot(THF)_4$ (orthorhombic, *Pbcn*), $\mathbf{2K_2}\cdot(THF)_4$ (monoclinic, $P2_1/n$), and $\mathbf{2Rb_2}\cdot(THF)_4$ (monoclinic, $P2_1/n$) in the solid state. Because of the similarity of all three structures, only $\mathbf{2Na_2}\cdot(THF)_4$ is plotted in Figure 6. In contrast to $\mathbf{2M_2}\cdot(DME)_3$ (M^+ = K^+, Rb^+, Cs^+) with their columnar structures, $\mathbf{2Na_2}\cdot(THF)_4$, $\mathbf{2K_2}\cdot(THF)_4$, and $\mathbf{2Rb_2}\cdot(THF)_4$ are arranged in a stepped formation. Much like $\mathbf{2M_2}\cdot(DME)_3$ (M^+ = K^+, Rb^+, Cs^+), each pyrazolyl substituent bridges two alkali metal ions. Unlike $\mathbf{2M_2}\cdot(DME)_3$ (M^+ = K^+, Rb^+, Cs^+), these ions are now symmetry-related and coordinated to two THF molecules. The most important difference in the crystal structures of $\mathbf{2M_2}\cdot(DME)_3$ (M^+ = Na^+, K^+, Rb^+, Cs^+) on one hand and $\mathbf{2M_2}\cdot(THF)_4$ (M^+ = Na^+, K^+, Rb^+) on the other arises from the way in which the M^+ ions are coordinated to the ferrocene fragments.

The THF complexes have each alkali metal ion bonded to one cyclopentadienyl ring only, which is reminiscent of the structural motif exhibited by the trimetallic aggregate $\mathbf{2Li_2}\cdot(DME)_2$ (Figure 3). In the DME complexes of the higher homologues, however, all M^+ ions are located in close proximity to two cyclopentadienyl rings. Moreover, the alkali metal ions in $\mathbf{2Na_2}\cdot(THF)_4$, $\mathbf{2K_2}\cdot(THF)_4$, and $\mathbf{2Rb_2}\cdot(THF)_4$ are shifted away from the center of the C_5H_4 ring toward the boryl substituent, which results in large differences between the individual $M^+\cdots$Cp(carbon) distances. The shortest contacts observed, Na(1)−C(15#) = 2.848(3) Å, K(1)−C(12) = 2.953(4) Å, and Rb(1)−C(12) = 3.156(12) Å, tend to be closer than the average $M^+\cdots$Cp(carbon) distances in the corresponding complexes

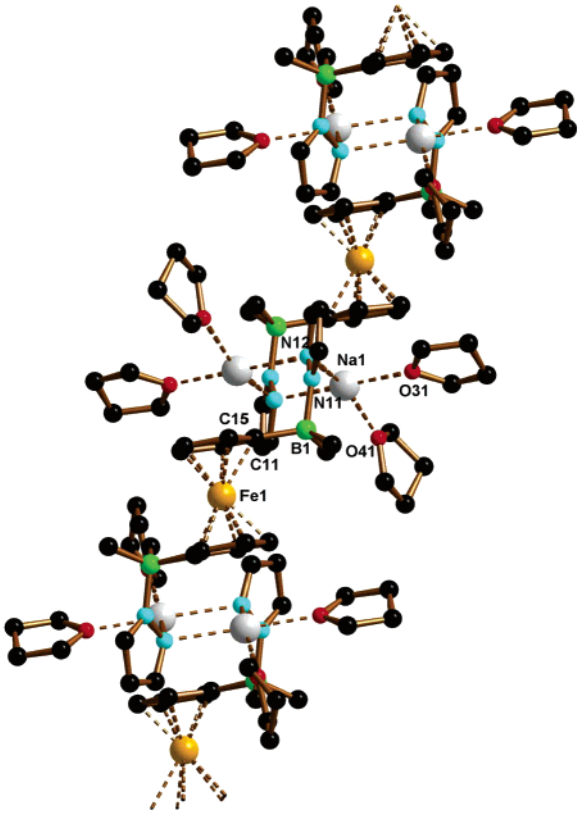

Figure 6. Molecular structure of $\mathbf{2Na_2}\cdot(THF)_4$ (hydrogen atoms omitted for clarity): Na(1)−C(15#) = 2.848(3) Å; symmetry transformation used to generate equivalent atoms: $-x+1, -y+1, -z+1$ (#). Molecular structure of $\mathbf{2K_2}\cdot(THF)_4$: K(1)−C(12) = 2.953(4) Å. Molecular structure of $\mathbf{2Rb_2}\cdot(THF)_4$: Rb(1)−C(12) = 3.156(12) Å.

$\mathbf{2Na_2}\cdot(DME)_3$ (2.84(9) Å), $\mathbf{2K_2}\cdot(DME)_3$ (3.48(9) Å), and $\mathbf{2Rb_2}\cdot(DME)_3$ (3.50(4) Å).

DFT Calculations. So far, we have gathered evidence that the ligand $[\mathbf{2}]^{2-}$ is well-suited for the generation of low-dimensional solids featuring stacks of alternating Fe(II)- and alkali metal cations sandwiched between cyclopentadienyl rings. In the next step, it has to be investigated whether this structural motif is merely due to crystal packing effects or whether alkali metal cation−ferrocene π interactions do play a major role. We therefore performed DFT calculations on the model complexes **5M**, $\mathbf{6M_2}$ (M^+ = Li^+, Na^+, K^+, Rb^+; Chart 1), and **7M** (M^+ = Li^+, Na^+, K^+; Chart 1) to get insight into the gas-phase geometries and binding enthalpies of alkali metal cation−η^5(ferrocene) complexes not perturbed by negatively charged substituents or the presence of adjutant sidearms. However, before elaborating further our effort to obtain theoretical data on cation−ferrocene π interactions, some discussion is in order for the corresponding cation−benzene π complexes, which have been studied in detail both by theoretical means[27,28] and experimentally by various gas-phase techniques.[27,29−31] Let us first consider the energy optimized structures of M^+(benzene) (**3M**, C_{6v}, M^+ = Li^+, Na^+, K^+, Rb^+, Cs^+; Chart 1) and

(26) Honeyman, G. W.; Kennedy, A. R.; Mulvey, R. E.; Sherrington, D. C. *Organometallics* **2004**, *23*, 1197−1199.

(27) Amicangelo, J. C.; Armentrout, P. B. *J. Phys. Chem. A* **2000**, *104*, 11420−11432.
(28) Feller, D.; Dixon, D. A.; Nicholas, J. B. *J. Phys. Chem. A* **2000**, *104*, 11414−11419.
(29) Woodin, R. L.; Beauchamp, J. L. *J. Am. Chem. Soc.* **1978**, *100*, 501−508.
(30) Sunner, J.; Nishizawa, K.; Kebarle, P. *J. Phys. Chem.* **1981**, *85*, 1814−1820.
(31) Armentrout, P. B.; Rodgers, M. T. *J. Phys. Chem. A* **2000**, *104*, 2238−2247.

Chart 1. Schematic Representations of the Alkali Metal Ion−Benzene Complexes **3M**, **4M**, and of the Alkali Metal Ion−Ferrocene Complexes **5M**, **6M$_2$**, **7M**, **8Li**, and **9Li**

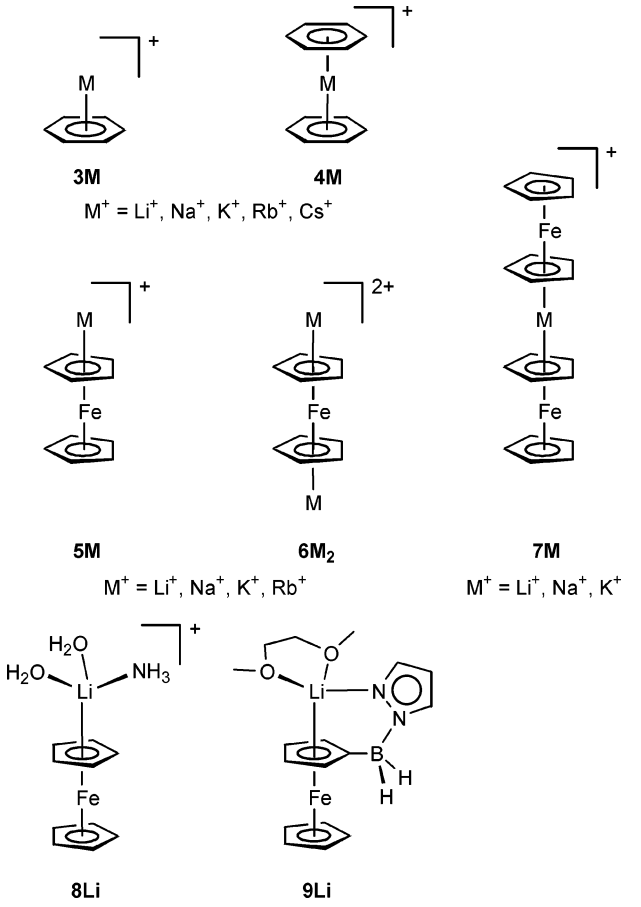

$M^+(benzene)_2$ (**4M**, D_{6h}, $M^+ = Li^+$, Na^+, K^+, Rb^+, Cs^+; Chart 1) and compare them with the geometries obtained by X-ray crystal structure analysis of $\mathbf{2M_2}\cdot(DME)_x$ ($M^+ = Li^+$, Na^+, K^+, Rb^+, Cs^+; $x = 2$, 3) as well as by our DFT calculations on the respective model complexes (Chart 1).

The most revealing structural feature, the $M^+\cdots$COG(benzene) and $M^+\cdots$COG(cyclopentadienyl) distances, are compiled in Table 1.

The $M^+\cdots$COG(benzene) contacts in **3M**, as calculated by Feller[28] and Armentrout[27] (Table 1), are consistently smaller than the sum of the half-thickness of benzene (1.7 Å)[3] and the ionic radii[6] of Li^+ (0.60 Å + 1.7 Å = 2.30 Å), Na^+ (0.95 Å + 1.7 Å = 2.65 Å), K^+ (1.33 Å + 1.7 Å = 3.03 Å), Rb^+ (1.48 Å + 1.7 Å = 3.18 Å), and Cs^+ (1.66 Å + 1.7 Å = 3.36 Å; note that the values employed for these calculations are at the lower limit of the alkali metal ion radii given by Shannon[32]). The difference between the $M^+\cdots$COG(benzene) distances (cf. the first two columns of Table 1) and the van der Waals contacts of M^+ and benzene (cf. the third column of Table 1) decreases monotonically from **3Li** to **3Cs**. This structural feature indicates the $M^+-\pi$ interaction to be disproportionately larger for the smaller alkali metal cations. The $M^+\cdots$COG(benzene) distances in the monobenzene complexes **3M** and in the dibenzene sandwich compounds **4M** are very similar.[27] The largest deviations are found for **3Li** (1.842 Å)/**4Li** (1.917 Å), which show a 4% increase of the $M^+\cdots$COG(benzene) distance upon complexation of the second benzene ring, and **3Rb** (3.165 Å)/**4Rb** (3.105 Å), where a 2% decrease is observed. In the case of **4Li**−**4K**, the somewhat larger $M^+\cdots$COG(benzene) contacts may be due to intramolecular steric repulsion of the two benzene rings, which becomes smaller with increasing size of the central metal ion. Michl et al. recently determined the crystal structures of $[M(benzene)_2]^+[CB_{11}Me_{12}]^-$ ($M^+ = Na^+$, K^+, Rb^+, Cs^+).[33] The crystals containing K^+, Rb^+, and Cs^+ are isomorphous with the metal cations being apically η^6-coordinated to two disordered, symmetry equivalent, nearly parallel benzene molecules in an essentially linear arrangement (COG−M^+−COG = 180 ± 3°) with $M^+\cdots$COG(benzene) distances of 3.14 Å (K^+), 3.19 Å (Rb^+), and 3.28 Å (Cs^+). Even though the structures of $[M(benzene)_2]^+$ in the condensed phase are influenced by the presence of the counterions as well as by crystal packing forces, the measured data are in reasonably good agreement with the $M^+\cdots$COG(benzene) distances calculated for **4M** (K^+, 2.832/2.917 Å, Rb^+, 3.105 Å, Cs^+, 3.392 Å; Table 1). Interestingly, compound $[Na(benzene)_2]^+[CB_{11}Me_{12}]^-$ adopts a different geometry in the solid state because it is coordinated to two benzene molecules in a tilted-sandwich arrangement (dihedral angle between the benzene rings: 55.9°) with distances $Na^+\cdots$COG(benzene) of 2.69 Å and 2.71 Å (cf. **4Na**: 2.421 Å). A similar structural motif as in $[Na(benzene)_2]^+[CB_{11}Me_{12}]^-$ has also been observed in the compound $[Na(toluene)_2]^+[Al(SiMe_3)_4]^-$ (dihedral angle between the toluene ligands: 61.6°).[34] Other useful data for comparison are provided by the X-ray crystal structure analyses of the salts $K[B(C_6H_5)_4]$[35] and $Rb[B(C_6H_5)_4]$,[36] because they give insight into π interactions between alkali metal cations and an arene equipped with an anionic borate substituent reminiscent of the borate sidearm of $[\mathbf{2}]^{2-}$. In both crystal structures, the respective alkali metal ion is embedded between two phenyl rings of the tetraphenyl borate anion at a distance of $M^+\cdots COG(C_6H_5)$ = 2.986 Å (average value K^+) and 3.060 Å (average value Rb^+).

Turning to the alkali metal cation−η^5(ferrocene) compounds **5M** (C_{5v}), we find that the π contacts calculated on the B3LYP//DZ level of theory tend to be slightly larger than the values obtained with the same hybrid functional and a basis set of triple-ζ quality (cf. Table 1). Moreover, the $M^+\cdots$COG(benzene) distances in **3M** and the $M^+\cdots$COG(cyclopentadienyl) distances in **5M** are pretty much alike. In this context, it is important to compare the theoretically obtained data for **3M** and **5M** with the experimentally determined values in Honeyman's cation[26] $[K(ferrocene)_2(toluene)_2]^+$, featuring $K^+\cdots\pi$ interactions to ferrocene ($M^+\cdots$COG(cyclopentadienyl): mean value = 2.964 Å) and toluene ($M^+\cdots COG(C_6H_5)$: mean value = 3.143 Å) in the same molecule. For the K^+−ferrocene fragment, the difference between the theoretical and experimental results is only 0.131 Å (ca. 5%; DZ basis set) and 0.161 Å (ca. 6%; TZ basis set). Larger discrepancies are observed for the K^+−toluene fragment (between 0.247 Å (ca. 9%) and 0.357 Å (ca. 13%) depending on the level of theory applied). Given the fact that

(32) Shannon, R. D. *Acta Crystallogr., Sect. A* **1976**, *32*, 751−767.

(33) King, B. T.; Noll, B. C.; Michl, J. *Collect. Czech. Chem. Commun.* **1999**, *64*, 1001−1012.
(34) Rösch, L.; Altnau, G.; Krüger, C.; Tsay, Y. H. *Z. Naturforsch., B: Chem. Sci.* **1983**, *38*, 34−41.
(35) Hoffmann, K.; Weiss, E. *J. Organomet. Chem.* **1974**, *67*, 221−228.
(36) Pajzderska, A.; Maiuszynska, H.; Wasicki, J. *Z. Naturforsch.* **2002**, *57a*, 847−853.

Table 1. Distances $M^+\cdots$COG [Å] between the Alkali Metal Ions M^+ and the Centroid (COG) of the Coordinated Benzene or Cyclopentadienyl Ring [B3LYP Hybrid Functional, Double-ζ (DZ) and Triple-ζ (TZ) Basis Sets]

M	**3M**[a]	**3M**[d]	$r(M^+)$ +1.7 Å[g]	**4M**[d]	**5M** DZ	**5M** TZ	**6M$_2$** DZ	**6M$_2$** TZ	**7M** DZ	**2M$_2$** exptl.[h]
Li	1.879[b]	1.842[e]	2.30	1.917[e]	1.870	1.837	2.018	1.971	1.995	2.35
Na	2.390[b]	2.394[e]	2.65	2.421[e]	2.350	2.350	2.506	2.518	2.427	2.576
K	2.786[b]	2.810[e]	3.03	2.832[e]	2.833	2.803	3.060	3.030	2.903	3.263
	2.786[c]	2.896[e,f]		2.917[e,f]						
Rb	3.100[c]	3.165[e,f]	3.18	3.105[e,f]	3.147		3.478			3.275
Cs	3.313[c]	3.417[e,f]	3.36	3.392[e,f]						3.283

[a] Reference 28. [b] MP2/CBS. [c] MP2/aVQZ. [d] Reference 27. [e] MP2(full)/6-311+G*. [f] The Hay−Wadt ECP/valence basis set was used for the metal atom. [g] Sum of the ionic radius of M^+ and the half-thickness of benzene. [h] Mean experimental value.

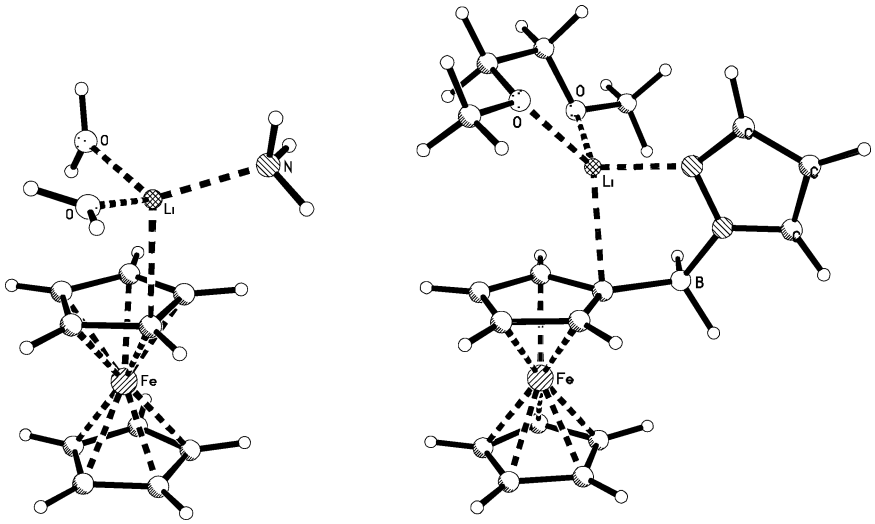

Figure 7. Optimized gas-phase structures of **8Li** (left) and **9Li** (right); B3LYP/TZ level of theory.

any cation−π interaction in $[K(ferrocene)_2(toluene)_2]^+$ is certainly hampered by steric crowding absent in the model complexes **3M** and **5M**, the larger experimental distances are not surprising (note that the toluene ligands coordinate to K^+ in a limited η^3 manner, which leads to a larger $M^+\cdots$COG-(C_6H_5) distance even though the potassium ion approaches C_{meta} (average distance: 3.331 Å) and C_{para} (average distance: 3.247 Å) of the toluene ring rather closely). All in all, we note a pleasingly good agreement between theory and experiment, which leads to the conclusion that the level of theory applied for the description of our alkali metal ion−η^5(ferrocene) interactions is adequate and leads to reliable structure predictions.

As in **3M**, the $M^+\cdots$COG(cyclopentadienyl) distances in **5M** are smaller than the calculated van der Waals contacts, and this feature is most pronounced for the smaller alkali metal ions (we assume that the half thickness of benzene equals the half thickness of the Cp ring in ferrocene). Coordination of a second ferrocene molecule to the same alkali metal ion (**7M**; D_{5h}) causes a small increase in the $M^+\cdots$COG(cyclopentadienyl) contacts of about 7% (**7Li**), 3% (**7Na**), and 2% (**7K**; Table 1) as has already been observed upon going from **3Li**−**3K** to **4Li**−**4K**. $M^+\cdots$COG(cyclopentadienyl) distances do also increase upon addition of a second metal ion to the same ferrocene moiety (cf. **6M$_2$**; D_{5h}). In this case, however, the degree of bond stretching is rather independent from the nature of the alkali metal ion (i.e., 8−10% upon going from **5M** to **6M$_2$**).

The molecular structure of the experimentally accessible system **2Li$_2$**·$(DME)_2$ is best compared with the hypothetical gas-phase aggregate **6Li$_2$**. The measured $Li^+\cdots$COG(cyclopentadienyl) distance of 2.35 Å (Table 1) is significantly longer than the corresponding value calculated for **6Li$_2$** (2.018 Å, DZ basis set; 1.971 Å, TZ basis set). In **2Na$_2$**·$(DME)_3$, the experimentally obtained $Na^+\cdots$COG(cyclopentadienyl) contact of 2.576 Å (Table 1) fits nicely to the corresponding distances in **6Na$_2$** (2.506 Å, DZ basis set; 2.518 Å, TZ basis set) and **7Na** (2.427 Å; note that the dihedral angle $Cp(Fc^1)//Cp(Fc^2)$ is 0° in the case of **7Na**, but 48.0° in **2Na$_2$**·$(DME)_3$, which is, however, not likely to have a large impact on the $Na^+\cdots$COG-(cyclopentadienyl) distances because alkali metal ions are essentially featureless spheres). The potassium ions in **2K$_2$**·$(DME)_3$ ($K^+\cdots$COG(cyclopentadienyl) = 3.263 Å; Table 1) are slightly further apart from the ferrocene cyclopentadienyl rings (7−9% deviation) than in the model complexes **6K$_2$** (3.060 Å/3.030 Å) and **7K** (2.903 Å). In contrast, somewhat shorter $Rb^+\cdots$COG(cyclopentadienyl) contacts are found in **2Rb$_2$**·$(DME)_3$ (3.275 Å) as compared to **6Rb$_2$** (3.478 Å). Apart from these subtle differences, both the absolute experimental values and the general trends upon variation of the alkali metal cation are very well reproduced by density functional theory, especially if one takes into account that gas-phase structures are compared with condensed-phase structures.

To get insight into the effects of Lewis-base coordination on the structural properties of $M^+\cdots\eta^5$(ferrocene) complexes, we have calculated the systems **8Li** and **9Li** (Chart 1, Figure 7). As to be expected, the $Li^+\cdots$COG(cyclopentadienyl) distance increases substantially upon going from **5Li** (1.870 Å, DZ basis set; 1.837 Å, TZ basis set) to **8Li** (2.915 Å, DZ basis set) and **9Li** (2.715 Å, DZ basis set). Thus, these calculated distances reproduce the qualitative trend very well even though the

Table 2. M^+(benzene) and M^+(ferrocene) Binding Enthalpies [kcal/mol]

M	**3M** ΔH_0[a]	**3M** ΔH_0[b]	**4M** ΔH_0[c]	**5M** ΔH_0[d]	**5M** ΔH_0[e]	**6M$_2$** ΔH_0[f]	**6M$_2$** ΔH_0[g]	**7M** ΔH_0[h]
Li	−36.1	−38.5 ± 3.2	−24.9 ± 1.6	−44.0	−45.3	26.4	25.6	−27.7
Na	−24.2	−22.1 ± 1.4	−19.1 ± 1.4	−30.0	−29.5	27.9	28.0	−21.8
K	−20.0	−17.5 ± 0.9	−16.1 ± 1.6	−20.1	−20.3	28.6	29.0	−15.9
Rb	−16.3	−16.4 ± 0.9	−15.0 ± 1.8	−14.8		24.7		
Cs	−12.4	−15.4 ± 1.1	−14.0 ± 1.8					

[a] Theoretical value according to ref 28, CCSD(T)/est. CBS. [b] Experimental value obtained from CID measurements according to ref 27. [c] Experimental value for the reaction **3M** + C_6H_6 → **4M**.[27] [d] B3LYP hybrid functional, double-ζ (DZ) basis set. [e] B3LYP hybrid functional, triple-ζ (TZ) basis set. [f] Theoretical value for the reaction **5M** + M^+ → **6M$_2$**, B3LYP hybrid functional, double-ζ (DZ) basis set. [g] Theoretical value for the reaction **5M** + M^+ → **6M$_2$**, B3LYP hybrid functional, triple-ζ (TZ) basis set. [h] Theoretical value for the reaction **5M** + $(C_5H_5)_2Fe$ → **7M**, B3LYP hybrid functional, double-ζ (DZ) basis set.

absolute values of the calculated Li^+···COG(cyclopentadienyl) distances are considerably larger than those observed in **2Li$_2$**·$(DME)_2$ (2.255−2.505 Å; mean value: 2.35 Å). Moreover, the lithium ion is shifted away from the center of the cyclopentadienyl ring (**8Li**, Li−COG−Fe = 149.7°; **9Li**, Li−COG−Fe = 147.3°). These shifts are most likely not associated with significant energy changes given the fact that the Li−COG−Fe angles in the four crystallographically independent molecules of **2Li$_2$**·$(DME)_2$ cover a range from 175.0° to 155.8°.

Binding enthalpies of **3M** (M^+ = Li^+, Na^+, K^+, Rb^+, Cs^+) at 0 K (ΔH_0) in the complete basis set limit[28] are compiled in Table 2. These values agree well with experimental data determined by collision-induced dissociation (CID) of **3M** with Xe in a guided ion beam mass spectrometer[27] (Table 2, second column). Experimental bond dissociation enthalpies for the respective bisbenzene complexes **4M** are also available[27] (Table 2, third column). The investigations on alkali metal−benzene complexes can be summarized as follows: (i) Bond dissociation enthalpies M^+−benzene as well as (benzene)M^+−benzene decrease monotonically with increasing size of M^+. (ii) CID experiments on **4M** indicate that the benzene rings are lost sequentially. The second benzene ring is generally less tightly bound to the metal ion than the first benzene ligand (Table 2); however, the difference between the first and the second dissociation enthalpy decreases along the sequence **4Li**/**3Li** to **4Cs**/**3Cs**. (iii) Comparisons drawn between the bond dissociation enthalpies of **3M**/**4M** on one hand and alkali metal−water complexes $M^+(H_2O)_x$ (x = 1, 2) on the other reveal comparable ΔH_0 values when M^+ = Li^+, Na^+, K^+ and larger bond dissociation enthalpies for **3M**/**4M** when M^+ = Rb^+, Cs^+.

Bond dissociation enthalpies for the alkali metal−ferrocene aggregates **5M** follow the same general trend as described for the alkali metal−benzene complexes **3M** (Table 2). By far, the most pronounced interaction is thus predicted for **5Li** (ΔH_0 = −44.0 kcal/mol, DZ basis set; ΔH_0 = −45.3 kcal/mol, TZ basis set), while Rb^+ bonding to ferrocene is considerably weaker (ΔH_0 = −14.8 kcal/mol, DZ basis set). In the case of **5Li** and **5Na**, the bond dissociation enthalpies are significantly higher than in the corresponding benzene complexes **3Li** and **3Na**, which indicates ferrocene to be superior over benzene as ligand to these alkali metal ions. Addition of a second ferrocene molecule to **5M** is exothermic by −27.7, −21.8, and −15.9 kcal/mol for Li^+, Na^+, and K^+, respectively. As in the case of the benzene aggregates, the second ferrocene ligand generally appears to be less strongly bound to the alkali metal ion than the first one. The reaction of a second alkali metal ion M^+ with **5M** to give **6M$_2$** is strongly endothermic (ΔH_0 = 26.4, 27.9, 28.6, and 24.7 kcal/mol for **6Li$_2$**, **6Na$_2$**, **6K$_2$**, and **6Rb$_2$**, respectively; DZ basis set). One obvious reason is that introduction of the additional positive charge leads to Coulomb repulsion within the molecule. Because the ferrocene-based ligand $[\mathbf{2}]^{2-}$ is equipped with two anionic substituents, destabilization of the aggregates **2M$_2$** due to unfavorable electrostatic interactions is probably not a major issue.

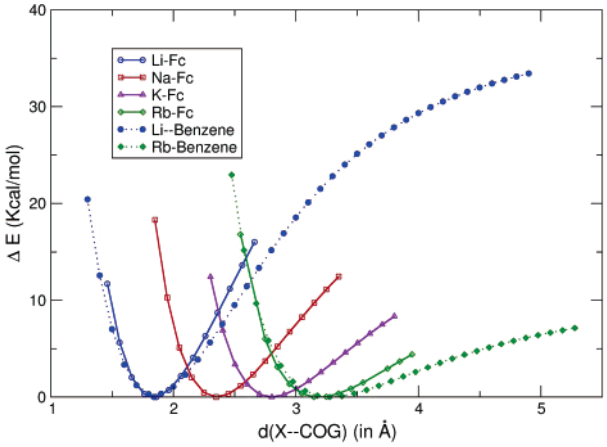

Figure 8. Potential energy curves of the M^+−ferrocene (**5M**) and Li^+/Rb^+−benzene (**3Li**/**3Rb**) complexes over the M···COG coordinate at the B3LYP/TZ level of theory (DZ basis and pseudopotentials for Rb complexes).

So far, it became evident that both the structural characteristics (e.g., M^+···COG distances) and the thermodynamic features (i.e., ΔH_0 values) of M^+···(benzene) and M^+···(ferrocene) complexes resemble each other. The question thus arises, whether the nature of the interaction of an alkali metal ion with benzene and the ferrocene cyclopentadienyl ring is also similar. The potential energy curves of **5Li**−**5Rb** together with those of **3Li** and **3Rb** calculated at the same level of theory are plotted in Figure 8. The largest differences between the shape of the potential energy surfaces of (i) **3Li**/**5Li** and (ii) **3Rb**/**5Rb** are apparent at longer M^+···COG distances, where the M^+···η^6(benzene) potential appears to be softer (cf. to stretch the optimal Li^+···COG(cyclopentadienyl) contact by 0.5 Å, an energy input of 9 kcal/mol is required, 3.8 kcal/mol more than in the case of Li^+···COG(benzene)).

It is widely accepted that, to first order, the binding sequence of Li^+−Cs^+ to benzene represents a classical electrostatic trend and that the cation interacts with the large permanent quadrupole moment of the aromatic.[2] As a rough estimate for **3Na**, 60% of the binding is due to electrostatics.[37]

Even though a purely electrostatic model is thus not valid to explain the absolute values of cation−π interactions, variations in ion-binding energies across a series of different π donor

(37) Mecozzi, S.; West, A. P., Jr.; Dougherty, D. A. *J. Am. Chem. Soc.* **1996**, *118*, 2307−2308.

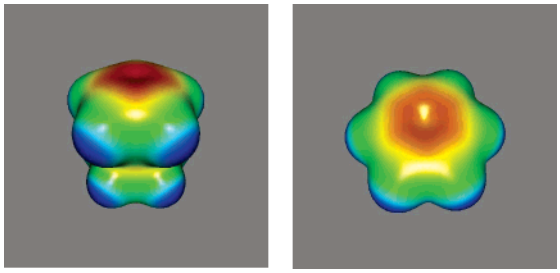

Figure 9. Electrostatic potential surface (EPS) of ferrocene (left) and benzene (right). The surfaces are calculated at the B3LYP/TZ level of theory, with a contour value of 0.02 bohr^{-3}. The colors represent the following energies (in kcal/mol): red < −19 kcal/mol, yellow = −9 kcal/mol, green = 0.0 kcal/mol, light-blue = +9 kcal/mol, blue > 19 kcal/mol.

molecules are faithfully mirrored by the electrostatic term.[2] Interestingly, the well-known aromatic substituent effects derived from studies of electrophilic aromatic substitution reactions (Hammett parameters) fail to provide a reliable tool for the prediction of trends in cation−π interactions. For example, even though phenol is much more prone to electrophilic attack than benzene, it turns out not to be superior when it comes to alkali metal ion binding.[2] Dougherty managed to rationalize differences in the degree of cation−π binding among selected aromatics by an inspection of their electrostatic potential surfaces (EPS): The more negative was the maximum electrostatic potential above the center of the aromatic, the stronger was the M$^+$···arene interaction.[7] We therefore calculated the EPS of ferrocene and benzene (B3LYP, TZ basis set) to see whether the higher ΔH_0 values obtained for compounds **5M** as compared to **3M** can be assigned to differences in the electrostatic potential of the two ligands. The EPSs of ferrocene and benzene are shown in Figure 9. There is a clear similarity between the two, but ferrocene has more negative charge localized at the center of the ring. The largest density at the given contour value, calculated at the B3LYP/TZ level of theory, corresponds to −17.3 kcal/mol for ferrocene and −14.6 kcal/mol for benzene.

For the fragment {[Fe(C$_5$H$_5$)$_2$]$_2$Ga}$^+$, our previous DFT calculations[15] indicated a transfer of 0.4 electrons into the gallium 4p orbitals. In contrast, the natural charges[38,39] of the alkali metal ions in **5M** and **7M** are uniformly close to +1 with the largest deviations being found for **5Li** (0.97) and **7Li** (0.93). This population analysis thus adds further support to the proposition that the interaction between M$^+$ and ferrocene is mainly electrostatic. However, the nature of the bonding will most likely change when the alkali metal ions are replaced by transition metal ions, because now d orbital contributions may lead to a more covalent interaction.

Conclusions

The alkali metal salts **2M$_2$** (M$^+$ = Li$^+$, Na$^+$, K$^+$, Rb$^+$, Cs$^+$) of the ditopic mono(pyrazol-1-yl)borate ligand [1,1′-fc(BMe$_2$-pz)$_2$]$^{2-}$, [**2**]$^{2-}$, crystallize from dimethoxyethane as multiple-decker sandwich complexes **2M$_2$**·(DME)$_x$ with alkali metal ions bound to the π faces of the ferrocene cyclopentadienyl rings in an η^5 manner. X-ray crystallographic analysis of **2Li$_2$**·(DME)$_2$ revealed discrete trinuclear complexes in which each lithium ion interacts with only one cyclopentadienyl ring. In contrast, infinite zigzag chains are formed by **2Na$_2$**·(DME)$_3$ in the solid state. Here, each sodium ion bridges the cyclopentadienyl rings of two different ferrocene moieties, whereas each cyclopentadienyl ring is coordinated by Fe(II) at one π face and by Na$^+$ at the other. The polyanionic charge of the macromolecular backbone is counterbalanced by [Na(DME)$_3$]$^+$ complexes. **2K$_2$**·(DME)$_3$, **2Rb$_2$**·(DME)$_3$, and **2Cs$_2$**·(DME)$_3$ establish very similar crystal structures consisting of linear columns [−CpR−Fe−CpR−M$^+$−CpR−Fe−CpR−M$^+$−]$_\infty$ (R = [−BMe$_2$pz]$^-$). We speculate that one reason for the different solid-state structures established by **2Li$_2$**·(DME)$_2$, **2Na$_2$**·(DME)$_3$, and **2K$_2$**·(DME)$_3$ lies in the ionic radii of the constituent alkali metal ions. When in a linear aggregate of the form CpFeCp···K$^+$···CpFeCp the potassium ion is replaced by a sodium ion, the distance between the cyclopentadienyl rings of the two coplanar coordinating ferrocene fragments is reduced by about 0.95 Å (cf. Table 1: calculated M$^+$···COG distances in **7K** (2.903 Å) and **7Na** (2.427 Å); COG, centroid of the cyclopentadienyl ring). Due to the presence of the [−BMe$_2$pz]$^-$ substituents in the real system **2M$_2$**·(DME)$_3$, a substitution of Na$^+$ for K$^+$ would thus lead to severe steric congestion between adjacent [**2**]$^{2-}$ ligands. This problem can be overcome when the coordination polymer is bent, which allows more space for the pyrazolyl rings but still maintains two energetically favorable cation−π bonds per sodium ion. In the case of **2Li$_2$**·(DME)$_2$, the yet smaller radius of the lithium ion is no longer compatible with the simultaneous coordination of two ligands [**2**]$^{2-}$ so that only a trinuclear aggregate is formed (cf. Table 1: calculated M$^+$···COG distances in **5Li** (1.837/1.870 Å) and **7Li** (1.995 Å)). Thus, the structural characteristics of **2Li$_2$**·(DME)$_2$, **2Na$_2$**·(DME)$_3$, and **2K$_2$**·(DME)$_3$ provide some experimental evidence that cation−π interactions are operative in these compounds because otherwise the M$^+$ radii and the M$^+$···COG distances would not be structure-determining factors.

DFT calculations on M$^+$···η^5(ferrocene) complexes **5M** in the gas phase give binding enthalpies of ΔH_0 = −44.0, −30.0, −20.1, and −14.8 kcal/mol for **5Li**, **5Na**, **5K**, and **5Rb**, respectively (B3LYP, double-ζ basis set; Chart 1, Table 2). In the case of **5Li** and **5Na**, these enthalpies are significantly larger than the values calculated for the corresponding M$^+$···η^6-(benzene) complexes **3Li** (ΔH_0 = −36.1 kcal/mol) and **3Na** (ΔH_0 = −24.2 kcal/mol; Chart 1, Table 2).[28] A comparison of **5K** (ΔH_0 = −20.1 kcal/mol)/**3K** (ΔH_0 = −20.0 kcal/mol)[28] and **5Rb** (ΔH_0 = −14.8 kcal/mol)/**3Rb** (ΔH_0 = −16.3 kcal/mol),[28] however, reveals cation−π interactions of similar strength in the ferrocene and benzene aggregates (note that the calculated binding enthalpies of **3Li**−**3Rb** are in nice agreement with experimentally determined ΔH_0 values[27] for these complexes). We therefore conclude that ferrocene is not only able to establish strong M$^+$···η^5(cyclopentadienyl) interactions to alkali metal ions but that to Li$^+$ and Na$^+$ it presents an even more attractive π face than benzene. This view is supported by an inspection of the electrostatic potential surfaces of ferrocene and benzene, because the strongest attraction of a pointlike +1 probe charge at the given contour value is −17.3 kcal/mol for ferrocene and −14.6 kcal/mol for benzene (B3LYP, triple-ζ basis set, Figure 9). For a full understanding as to why the lighter alkali metal ions show a stronger preference for ferrocene than their heavier homologues, further investigations will be required. Looking at the mean experimental M$^+$···COG distances in **2M$_2$**·

(38) Reed, A. E.; Curtiss, L. A.; Weinhold, F. *Chem. Rev.* **1988**, *88*, 899−926.
(39) Glendening, A. E.; Reed, A. E.; Carpenter, J. E.; Weinhold, F. *NBO Version 3.1.*

$(DME)_x$ (Li^+, 2.35 Å; Na^+, 2.576 Å; K^+, 3.263 Å; Rb^+, 3.275 Å; Cs^+, 3.283 Å) and the corresponding calculated distances in the model complexes **5M** (Li^+, 1.870 Å; Na^+, 2.350 Å; K^+, 2.833 Å; Rb^+, 3.147 Å), we find the $M^+\cdots$COG contacts in the real compounds to be longer. However, these bond stretches do not correspond to large energies. For example, even in the most strongly bound complex **5Li** an energy input of only 9 kcal/mol is required to increase the $Li^+\cdots$COG distance from the optimal (1.870 Å) to the experimentally determined value (2.35 Å). It is thus apparent that the ligand system $[\mathbf{2}]^{2-}$ is well-suited for the promotion of π interactions between metal atoms and the ferrocene cyclopentadienyl ring. Work is currently in progress to employ $[\mathbf{2}]^{2-}$ for the synthesis of multiple-decker sandwich complexes consisting of ferrocene and transition metal atoms, where a more pronounced metal−iron interaction along the polymer backbone may be envisaged.

Experimental Section

General Remarks. All reactions and manipulations of air-sensitive compounds were carried out in dry, oxygen-free nitrogen using standard Schlenk ware. Solvents were freshly distilled under argon from Na−benzophenone (diethyl ether, THF, DME) prior to use. NMR: Bruker Avance 400, Bruker DPX 250. ^{11}B NMR spectra are reported relative to external $BF_3{\cdot}Et_2O$; ^{7}Li NMR spectra are reported relative to external LiCl in D_2O. Unless stated otherwise, all NMR spectra were run at ambient temperature; abbreviations: s = singlet, d = doublet, vtr = virtual triplet, br = broad, n.r. = multiplet expected in the NMR spectrum but not resolved, n.o. = signal not observed. Compound **1**[40] was synthesized according to a literature procedure.

Preparation of $2Li_2$. A slurry of Lipz (0.34 g, 4.60 mmol) in Et_2O (15 mL) was added with stirring at −78 °C via a dropping funnel to **1** (0.61 g, 2.30 mmol) in Et_2O (15 mL). The mixture was slowly warmed to room temperature, whereupon a yellow-orange precipitate of $\mathbf{2Li_2}{\cdot}(Et_2O)_4$ formed (the number of ether solvate molecules was determined by integration of the ^{1}H NMR spectrum in d_8-THF). After filtration, the mother liquor was stored at 5 °C overnight to yield a second crop. Yield of $\mathbf{2Li_2}{\cdot}(Et_2O)_4$: 1.52 g (93%). X-ray quality crystals of $\mathbf{2Li_2}{\cdot}(DME)_2$ were obtained after a saturated solution of $\mathbf{2Li_2}{\cdot}(Et_2O)_4$ in DME had been stored at 5 °C over a period of several days. ^{11}B NMR (128.4 MHz, d_8-THF): δ −9.0 ($h_{1/2}$ = 300 Hz). ^{1}H NMR (400.1 MHz, d_8-THF): δ 0.11 (s, 12H, CH_3), 4.05, 4.19 (2 × vtr, 2 × 4H, $^3J_{HH} = {}^4J_{HH}$ = 1.6 Hz, C_5H_4), 5.95 (vtr, 2H, $^3J_{HH}$ = 1.9 Hz, pz-H4), 7.01, 7.48 (2 × d, 2 × 2H, $^3J_{HH}$ = 1.7, 2.0 Hz, pz-H3,5). ^{13}C NMR (100.6 MHz, d_8-THF): δ 12.8 (n.r., CH_3), 71.0, 72.2 (C_5H_4), 102.8 (pz-C4), 131.9, 135.4 (pz-C3,5), n.o. (C_5H_4−C*ipso*). ^{7}Li NMR (155.5 MHz, d_8-THF): δ −1.30 ($h_{1/2}$ = 37 Hz). Anal. Calcd for $\mathbf{2Li_2}{\cdot}(DME)_2$, $C_{28}H_{46}B_2FeLi_2N_4O_4$ (594.04): C, 56.61; H, 7.81; N, 9.43. Found: C, 56.33; H, 7.72; N, 9.09.

Preparation of $2Na_2$. A slurry of Napz (0.24 g, 2.70 mmol) in Et_2O (20 mL) was added with stirring via a dropping funnel at −78 °C to **1** (0.36 g, 1.35 mmol) in Et_2O (20 mL). The mixture was slowly warmed to room temperature, whereupon a yellow-orange precipitate formed which was isolated by filtration. The microcrystalline solid was dissolved in THF (20 mL), and the solution was stirred for 24 h and evaporated to dryness in vacuo to substitute THF for Et_2O in the coordination sphere of the Na^+ ions. Yield of $\mathbf{2Na_2}{\cdot}(THF)_4$: 0.94 g (95%). X-ray quality crystals of $\mathbf{2Na_2}{\cdot}(THF)_4$ formed from a saturated THF solution at −30 °C over a period of several days. X-ray quality crystals of $\mathbf{2Na_2}{\cdot}(DME)_3$ formed from a saturated solution of $\mathbf{2Na_2}{\cdot}(THF)_4$ in DME at −30 °C over a period of several days.

^{11}B NMR (128.4 MHz, d_8-THF): δ −9.1 ($h_{1/2}$ = 250 Hz). ^{1}H NMR (400.1 MHz, d_8-THF): δ 0.03 (s, 12H, CH_3), 3.86, 3.98 (2 × n.r., 2 × 4H, C_5H_4), 5.84 (n.r., 2H, pz-H4), 6.99, 7.44 (2 × n.r., 2 × 2H, pz-H3,5). ^{13}C NMR (100.6 MHz, d_8-THF): δ 13.2 (br, CH_3), 69.3, 72.0 (C_5H_4), 101.9 (pz-C4), 131.7, 136.2 (pz-C3,5), n.o. (C_5H_4−C*ipso*). Anal. Calcd for $\mathbf{2Na_2}{\cdot}(DME)_3$, $C_{32}H_{56}B_2FeN_4Na_2O_6$ (716.26): C, 53.66; H, 7.88; N, 7.82. Found: C, 53.38; H, 7.72; N, 7.49.

Preparation of $2K_2$. The compound was synthesized similar to $\mathbf{2Na_2}$ from Kpz (0.80 g, 7.54 mmol) and **1** (1.00 g, 3.76 mmol) in Et_2O (60 mL). Yield of $\mathbf{2K_2}{\cdot}(THF)_4$: 2.65 g (92%). Recrystallization of $\mathbf{2K_2}{\cdot}(THF)_4$ from hot THF afforded orange blocks suitable for single-crystal X-ray diffraction. To obtain X-ray quality crystals of $\mathbf{2K_2}{\cdot}(DME)_3$, $\mathbf{2K_2}{\cdot}(THF)_4$ was dissolved in DME at 40 °C in an ultrasonic bath and the resulting clear yellow-orange solution was slowly concentrated in vacuo. ^{11}B NMR (128.4 MHz, d_8-THF): δ −9.4 ($h_{1/2}$ = 250 Hz). ^{1}H NMR (400.1 MHz, d_8-THF): δ 0.11 (s, 12H, CH_3), 3.96, 4.00 (2 × vtr, 2 × 4H, $^3J_{HH} = {}^4J_{HH}$ = 1.5 Hz, C_5H_4), 5.85 (vtr, 2H, $^3J_{HH}$ = 1.4 Hz, pz-H4), 7.06, 7.48 (n.r., d, 2 × 2H, $^3J_{HH}$ = 1.9 Hz, pz-H3,5). ^{13}C NMR (62.9 MHz, d_8-THF): δ 13.2 (br, CH_3), 69.2, 73.2 (C_5H_4), 101.5 (pz-C4), 131.2, 136.1 (pz-C3,5), n.o. (C_5H_4−C*ipso*). Anal. Calcd for $\mathbf{2K_2}{\cdot}(DME)_3$, $C_{32}H_{56}B_2FeK_2N_4O_6$ (748.48): C, 51.35; H, 7.54; N, 7.49. Found: C, 51.26; H, 7.51; N, 7.19.

Preparation of $2Rb_2$. The compound was synthesized similar to $\mathbf{2Na_2}$ from Rbpz (1.00 g, 6.56 mmol) and **1** (0.87 g, 3.28 mmol) in Et_2O (50 mL). Yield of $\mathbf{2Rb_2}{\cdot}(THF)_4$: 2.64 g (94%). X-ray quality crystals of $\mathbf{2Rb_2}{\cdot}(THF)_4$ formed from a saturated THF solution at 5 °C over a period of several days. $\mathbf{2Rb_2}{\cdot}(THF)_4$ was dissolved in DME at 70 °C in an ultrasonic bath. After being cooled to room temperature, the clear yellow-orange solution was slowly concentrated in vacuo, whereupon orange platelets of $\mathbf{2Rb_2}{\cdot}(DME)_3$ formed.

^{11}B NMR (128.4 MHz, d_8-THF): δ −7.6 ($h_{1/2}$ = 370 Hz). ^{1}H NMR (400.1 MHz, d_8-THF): δ 0.14 (s, 12H, CH_3), 3.95 (n.r., 8H, C_5H_4), 5.87 (vtr, 2H, $^3J_{HH}$ = 1.6 Hz, pz-H4), 7.15, 7.49 (n.r., d, 2 × 2H, $^3J_{HH}$ = 1.6 Hz, pz-H3,5). ^{13}C NMR (100.6 MHz, d_8-THF): δ 12.9 (br, CH_3), 69.4, 73.1 (C_5H_4), 99.7 (br, C_5H_4−C*ipso*), 101.0 (pz-C4), 130.5, 135.7 (pz-C3,5). Anal. Calcd for $\mathbf{2Rb_2}{\cdot}(DME)_3$, $C_{32}H_{56}B_2FeN_4O_6Rb_2$ (841.22): C, 45.69; H, 6.71; N, 6.66. Found: C, 45.45; H, 6.59; N, 6.30.

Preparation of $2Cs_2$. The compound was synthesized similar to $\mathbf{2Na_2}$ from Cspz (0.78 g, 3.90 mmol) and **1** (0.52 g, 1.95 mmol) in Et_2O (45 mL). Because the crude product is only poorly soluble in THF, it was recrystallized from DME at 40 °C in an ultrasonic bath. Yield of $\mathbf{2Cs_2}{\cdot}(DME)_3$: 1.75 g (96%). ^{11}B NMR (128.4 MHz, d_8-THF): δ −7.6 ($h_{1/2}$ = 210 Hz). ^{1}H NMR (400.1 MHz, d_8-THF): δ 0.17 (s, 12H, CH_3), 3.94, 3.99 (2 × vtr, 2 × 4H, $^3J_{HH} = {}^4J_{HH}$ = 1.6 Hz, C_5H_4), 5.85 (vtr, 2H, $^3J_{HH}$ = 1.5 Hz, pz-H4), 7.13, 7.48 (n.r., d, 2 × 2H, $^3J_{HH}$ = 1.9 Hz, pz-H3,5). ^{13}C NMR (100.6 MHz, d_8-THF): δ 11.5 (br, CH_3), 70.1, 72.5 (C_5H_4), 100.9 (pz-C4), 130.1, 135.3 (pz-C3,5), n.o. (C_5H_4−C*ipso*). Anal. Calcd for $\mathbf{2Cs_2}{\cdot}(DME)_3$, $C_{32}H_{56}B_2Cs_2FeN_4O_6$ (936.10): C, 41.06; H, 6.03; N, 5.99. Found: C, 40.88; H, 6.10; N, 5.71.

X-ray Crystal Structure Analyses. The data collections for all structures were performed on a STOE IPDS-II two-circle diffractometer with graphite-monochromated Mo Kα radiation (λ = 0.71073). The structures were solved by direct methods using the program SHELXS[41] and refined by full-matrix least-squares calculations on F^2 using the program SHELXL97.[42] All absorption corrections were performed with the MULABS[43] option in PLATON.[44] All non-H atoms (with the exception of $\mathbf{2Li_2}{\cdot}(DME)_2$; see below) have been refined anisotropically, whereas the H atoms have been treated as riding atoms with their displacement parameters fixed to 1.2 or 1.5 (for methyl groups) of the value of their parent atom. The C atoms of $\mathbf{2Li_2}{\cdot}(DME)_2$ were restrained in a way that their U_{ij} components approximate to isotropic behavior. B and Li atoms were refined isotropically. The THF rings of $\mathbf{2Rb_2}{\cdot}(THF)_4$ were restrained to have equal bond lengths and angles. CCDC reference numbers: 246210 ($\mathbf{2Li_2}{\cdot}(DME)_2$), 246213 ($\mathbf{2Na_2}{\cdot}(DME)_3$),

(40) Ruf, W.; Renk, T.; Siebert, W. *Z. Naturforsch.* **1976**, *31b*, 1028−1034.

(41) Sheldrick, G. M. *Acta Crystallogr., Sect. A* **1990**, *46*, 467−473.
(42) Sheldrick, G. M. *SHELXL-97. A Program for the Refinement of Crystal Structures*; Universität Göttingen, 1997.
(43) Blessing, R. H. *Acta Crystallogr., Sect. A* **1995**, *51*, 33−38.
(44) Spek, A. L. *Acta Crystallogr., Sect. A* **1990**, *46*, C34.

246212 (**2K$_2$·**(DME)$_3$), 246211 (**2Rb$_2$·**(DME)$_3$), 246208 (**2Cs$_2$·**(DME)$_3$), 246207 (**2Na$_2$·**(THF)$_4$), 246206 (**2K$_2$·**(THF)$_4$), 246209 (**2Rb$_2$·**(THF)$_4$).

Electrochemistry. Cyclic voltammetry was performed in THF solutions containing [NBu$_4$][PF$_6$] (0.1 mol l^{-1}) as the supporting electrolyte. All potential values are reported relative to the FcH/FcH$^+$ redox couple. The cell for voltammetric studies was designed as detailed in ref 45. Voltammetric scans were referenced by addition of a small amount of ferrocene as internal standard at an appropriate time of the experiment.

Computational Details. Calculations were performed using Gaussian 98[46] and Gaussian 03[47] program packages. On the basis of our previous experience with similar systems,[9] we chose the B3LYP hybrid functional[48−50] together with basis sets of double-ζ quality (the DZVP basis set given by Salahub et al.[51,52] for iron and Pople's 6-31++G** for the rest of the atoms; this basis set combination will be denoted as DZ) to generate educated guesses for starting stationary points and reoptimization with triple-ζ quality basis sets. For iron, the TZVP basis given by Schäfer et al.[53] was employed, supplemented with a diffuse s function (with an exponent 0.33 times that of the most diffuse s function on the original set), two sets of p functions (optimized by Wachters)[54] for the excited states, one set of diffuse pure angular momentum d functions (optimized by Hay),[55] and three sets of uncontracted pure angular momentum f functions, including both tight and diffuse exponents, as recommended by Ragavachari and Trucks;[56] Pople's 6-311++G(2df,2p) basis was used for the rest of the atoms. This basis set will be hereafter denoted as TZ. As shown in Tables 1 and 2, both basis sets give similar results, which compare well with theoretical and experimental values available from other sources. Supported by the good agreement of data obtained at the DZ and TZ level of theory, the DZ basis set was used in the computations of the larger systems and all of the Rb containing structures (with the Hay and Wadt effective core pseudopotentials for Rb[57]). DFT methods are known to have smaller basis set superposition errors (BSSE) than other theoretical methods such as MP2.[58] Thus, combinations of DFT with large polarized basis functions (as the TZ used in the present manuscript) guarantee the BSSE to be negligible.[59] Nevertheless, because a DZ basis set is used in the largest molecules, the BSSE was evaluated for **7Na** (**7M** column of Table 2), and, as expected, the calculated value was very small (1.12 kcal/mol). All structures were verified to represent minima of the potential energy surface by vibrational frequency analysis. The zero-point vibrational energies ZPVEs were calculated in the rigid rotor-harmonic oscillator approximation. The rotational and translational energies were treated classically as $^1/_2RT$ per degree of freedom.

The electrostatic potentials (ESP, Figure 9) have been calculated on selected points F belonging to the isodensity surface with constant electron density $\rho(\bar{r}) = 0.02$ bohr^{-3} as

$$V(\bar{r}) = \int \frac{\rho(\bar{r}')}{|\bar{r} - \bar{r}'|}\, \mathrm{d}\bar{r}'$$

where the electron density has been written in terms of the $N/2$ lowest energy Kohn−Sham orbitals as

$$\rho(\bar{r}) = 2\sum_{i=1}^{N/2} \phi_i(\bar{r})\phi_i^*(\bar{r})$$

with N being the number of electrons of the system.

Acknowledgment. M.W. is grateful to the Deutsche Forschungsgemeinschaft (DFG) for financial support and to Chemetall for generous gifts of organolithium compounds. M.S. wishes to thank the Fonds der Chemischen Industrie (FCI) and the Bundesministerium für Bildung und Forschung (BMBF) for a Ph.D. grant. The SGI/ IZO-SGIker UPV/EHU (supported by European Social Fund and MCyT) is gratefully aknowledged by J.M.M, I.S., and J.M.U. for the generous allocation of computational resources.

Supporting Information Available: Absolute energies (in hartrees) and coordinates of the theoretically calculated structures **3Li**, **3Rb**, ferrocene, **5M**, **6M$_2$**, **7M**, **8Li**, **9Li**; full refs 46 and 47; selected crystallographic data together with bond lengths, angles, torsion angles, and dihedral angles of **2Li$_2$·**(DME)$_2$, **2M$_2$·**(DME)$_3$, and **2M$_2$·**(THF)$_4$; plots of the structures of **2Rb$_2$·**(DME)$_3$, **2Cs$_2$·**(DME)$_3$, **2K$_2$·**(THF)$_4$, and **2Rb$_2$·**(THF)$_4$; CIF files of all structures determined by X-ray crystallography. This material is available free of charge via the Internet at http://pubs.acs.org.

JA051544+

(45) Winter, R. F.; Hornung, F. M. *Organometallics* **1999**, *18*, 4005−4014.
(46) Pople, J. A.; et al. *Gaussian 98*, revision A.11; Gaussian, Inc.: Pittsburgh, PA, 1998.
(47) Pople, J. A.; et al. *Gaussian 03*, revision C.02; Gaussian, Inc.: Wallingford, CT, 2004.
(48) Becke, A. D. *Phys. Rev. A* **1988**, *38*, 3098−3100.
(49) Lee, C.; Yang, W.; Parr, R. G. *Phys. Rev. B* **1988**, *37*, 785−789.
(50) Becke, A. D. *J. Chem. Phys.* **1993**, *98*, 5648−5652.
(51) Sim, F.; Salahub, D. R.; Chin, S.; Dupuis, M. *J. Chem. Phys.* **1991**, *95*, 4317−4326.
(52) Godbout, N.; Salahub, D. R.; Andzelm, J.; Wimmer, E. *Can. J. Chem.* **1992**, *70*, 560−571.
(53) Schäfer, A.; Huber, C.; Ahlrichs, R. *J. Chem. Phys.* **1994**, *100*, 5829−5835.
(54) Wachters, A. J. H. *J. Chem. Phys.* **1970**, *52*, 1033−1036.
(55) Hay, P. J. *J. Chem. Phys.* **1977**, *66*, 4377−4384.
(56) Raghavachari, K.; Trucks, G. W. *J. Chem. Phys.* **1989**, *91*, 1062−1065.
(57) Hay, P. J.; Wadt, W. R. *J. Chem. Phys.* **1985**, *82*, 299−310.
(58) Andzelm, J.; Wimmer, E. *J. Chem. Phys.* **1992**, *96*, 1280−1303.
(59) Mercero, J. M.; Matxain, J. M.; López, X.; York, D. M.; Largo, A.; Eriksson, L. A.; Ugalde, J. M. *Int. J. Mass Spectrom.* **2005**, *240*, 37−99.